PROGRESS REPORT: GEOLOGIC VALIDATION OF EO-1 HYPERION USING AVIRIS

F. A. Kruse,[1] J. W. Boardman,[1] and J. H. Huntington[2]

1.0 Introduction

Over the last few years, the field of imaging spectrometry has grown rapidly as new instruments and analysis techniques have been developed. The launch of Hyperion as part of NASA's EO-1 program represents a significant landmark in the progression of the technology; the first spaceborne imaging spectrometry system. AIG, in cooperation with CSIRO, is evaluating, validating, and demonstrating use of EO-1 Hyperion hyperspectral data for geologic applications. The Airborne Visible/Infrared Imaging Spectrometer (AVIRIS) plays a pivotal role in this effort. This manuscript describes the geologic test sites being used and progress on preparing "ground truth" for anticipated Hyperion data collects using AVIRIS data. Preliminary findings are extrapolated to predict the effect of instrument characteristics and performance on geologic mapping using Hyperion.

2.0 EO-1 Hyperion Summary

Hyperion is a pushbroom/diffraction grating imaging spectrometer launched as part of NASA's EO-1 mission on 21 November 2000. The instrument has 200 spectral bands covering the 0.4 to 2.5 µm range with approximately 10nm spectral resolution and 30 meter spatial resolution. Ground coverage is approximately 7.5 km by 180 km per image (24 second collect). Signal-to-noise ratios are estimated as approximately 100:1 in the VNIR and 50:1 for the SWIR.

3.0 Objectives

Characterization and validation of Hyperion are key tasks in the understanding of its performance, its utility for specific applications, and the planning for future systems. The objectives of the AIG/CSIRO research are to evaluate Hyperion to determine its performance and to validate with respect to requirements for applied and commercial use of space-based hyperspectral data for geologic applications. We are evaluating, validating, and demonstrating Hyperion in the role of geologic mapping and in the context of monitoring the processes that control the occurrence of non-renewable mineral resources, especially mineral deposits. We are also examining the issues of spectral and spatial scaling using Hyperion data, using the data to examine parameters inherent to analysis of satellite hyperspectral data (subpixel detection, identification, quantification, and mapping). Our principle means of validating Hyperion is through comparison with airborne hyperspectral datasets (AVIRIS and HyMap), laboratory and field spectral measurements, and satellite simulations.

4.0 AIG Hyperion Geologic Validation Sites

Three primary test sites representing geologically diverse terrains are being used for the AIG/CSIRO Hyperion validation effort; the N. Grapevine Mountains, Nevada; Oatman, Arizona; and Virginia City, Nevada. Secondary sites in Argentina, Australia, Israel, and New Zealand are also being imaged. Existing AVIRIS/HyMap data and supporting information serve as the baseline for determination of Hyperion spectral, spatial and radiometric properties.

NGM Site: The northern Grapevine Mountains (NGM) site, located in south-central Nevada (Figure 1), consists of about one third of the "West of Gold Mountain" U.S. Geological Survey 7 1/2 minute quadrangle (1:24,000 scale). The site has been studied in detail using field mapping and several remote sensing data sets (Kruse, 1988; Kruse et al., 1993b; Kruse et al., 1999). Existing geologic maps include 1:62,500-scale bedrock mapping by (Wrucke et al., 1984) and mapping of surficial deposits by Moring (1986). More detailed site-specific mapping has also been performed (Kruse, 1988). The NGM site is ideal for Hyperion validation because of the presence of both large (disseminated) and small (vein) alteration zones, common alteration minerals with similar spectral signatures, and the abundance of supporting hyperspectral data (AIS/AVIRIS/HyMap).

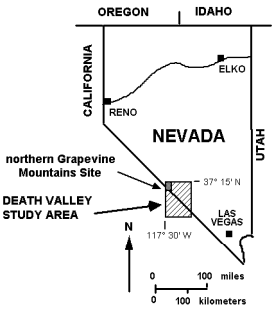

Figure 1: Location map

[1] Analytical Imaging and Geophysics, Boulder, Colorado 80303 (www.aigllc.com)

[2] CSIRO, Sydney, Australia

PreCambrian bedrock in the NGM area consists of limestones, dolomites, sandstones and their contact metamorphic equivalents, however, published geologic maps do not distinguish between the different lithologies. Mesozoic plutonic rocks are mapped primarily as granitic-composition and some age-dates are available (Albers and Stewart, 1972). Mesozoic units mapped in the field during previous investigations include quartz syenite, a quartz monzonite porphyry stock, quartz monzonite dikes, and a granite intrusion (Kruse, 1988). These rocks are cut by narrow north-trending mineralized shear zones containing sericite (fine grained muscovite or illite) and iron oxide minerals (Wrucke et al., 1984; Kruse, 1988). Slightly broader northwest-trending zones of disseminated quartz, pyrite, sericite, chalcopyrite, and fluorite mineralization (QSP alteration) ± goethite occur in the quartz monzonite porphyry. This type of alteration is spatially associated with fine-grained quartz monzonite dikes (Kruse, 1988). There are several small areas of quartz stockwork (silica flooding of the rocks) exposed at the surface in the center of the area, and skarn, composed mainly of brown andradite garnet near contact zones with limestone/dolomite. Complexly faulted, Tertiary volcanic rocks related to the Timber Mountain Caldera in southern Nevada are abundant around the southern periphery of the study area and are overlain by volcaniclastic sedimentary rocks interbedded with rhyolite and basalt (Wrucke et al., 1984). Quaternary deposits include Holocene and Pleistocene fanglomerates, pediment gravels, and alluvium.

Virginia City, Nevada: Virginia City is located in the Virginia Range in west-central Nevada, SE of Reno, Nevada. The Comstock Lode Mining District at Virginia City produced over 200 million oz of silver and 9 million oz of gold during the mid-1800s. The andesitic volcanic rocks that host the ore deposits are extensively altered and bleached. Zones of hydrothermal alteration are widely exposed and identifiable on Landsat MSS and TM images due to their light color and the presence of iron oxide and clay minerals (Hutsinpiller, 1988). Previous remote sensing studies of the Virginia City district have been made by Hutsinpiller, 1988, and Elvidge, 1985. Other studies have been made by Whitebread, 1976, and Thompson, 1956.

Virginia City was chosen as an Hyperion site because of the abundance of hydrothermal alteration minerals, existence of appropriate supporting hyperspectral data (AVIRIS/HyMap), the presence of one of the world's most valuable, historic mineral fields, complex and relatively poorly exposed geology and the complementary nature of the terrain to the other AIG/CSIRO sites. The area is rugged, well vegetated and encompasses extensive old (contaminating) mine activity, dumps and urban development, as well as natural fresh and altered outcrops. Virginia City thus represents a typical site that users of spaceborne hyperspectral data might encounter, more difficult than NGM in many respects, but one that we will have to learn to deal with.

The following geological summary is taken largely from Hutsinpiller (1988). The oldest rocks in the district are Mesozoic meta-sediments and meta-volcanics that have been intruded by Cretaceous granodiorite and granite. Unconformably overlying the Mesozoic rocks are a series of silicic ash-flow tuff. These are overlain by thick andesite flows and breccias of the Miocene Alta Formation, the main host of the orebodies in the district. Dikes and stocks of the Davidson Diorite intrude the Mesozoic rocks and the Alta Formation. Overlying the Alta Formation are andesitic to dacitic flows and associated dikes and stocks of the Kate Peak Formation. During emplacement of the lower member of the Kate Peak Formation normal faulting, mineralization and alteration occurred. The Knickerbocker Andesite unconformably overlies the Kate Peak Formation.

Mineralization and hydrothermal alteration in the Comstock Lode District are mostly confined to the northerly-trending Comstock, Silver City and Occidental fault zones, although some ore was mined in hanging wall faults. The faults dip moderately to the east but are nearly vertical at the surface. Post-mineral faulting has displaced the hanging-wall ore bodies as well as portions of the ore-bodies within the main fault zones. Hudson (1984) defines seven alteration assemblages at Virginia City (Table 1).

Alteration assemblages vary with depth from the palaeo-surface and horizontal distance form the major faults. At the surface, in the hanging wall, narrow alunitic and alsic ledges grade laterally into kaolinitic alteration. The kaolinite zones in turn grade into illitic and finally into propylitic alteration. Illitic and kaolinitic assemblages occur in zones from several meters to over 500 meters in width. Propylitically altered rocks of varying intensity are widespread throughout the district. Patches of sericitic alteration up to 800 meters wide crop out west of Virginia City in the footwall of the Comstock Fault.

Table 1 - Alteration Mineral Assemblages at Virginia City (from Hutsinpiller, 1988)

Alteration Type	Alteration Assemblage	Minerals with SWIR absorptions
Propylitic	albite, chlorite, epidote, calcite, white mica, (illite &/or sericite), quartz, pyrite	Chlorite, epidote, calcite, white mica
Illitic	Illite, quartz, pyrite, mixed-layer illite-montmorillonite	Illite, montmorillonite
Kaolinitic	Kaolinite, quartz, pyrite	Kaolinite
Alsic	Pyrophyllite, quartz, diaspore, kaolinite, pyrite	Pyrophyllite, kaolinite
Alunitic	Quartz, alunite, pyrite	Alunite
Sericitic	Sericite, quartz, pyrite	Sericite
Silicification	Quartz, adularia, calcite	Calcite

Thus it is apparent that many of the minerals we believe Hyperion will be able to map are present in the Virginia City area. It should be noted, however, that much of this information has been derived from detailed petrological work on drill hole samples and it is not clear how much of this mineralogical variety may be evident on the surface rocks, soils and exposures visible from above (as opposed to road-side cuttings).

Oatman, Arizona: The Oatman Mining District lies approximately 160 km south-east of Las Vegas Nevada, mid-way between Needles, California and Kingman, Arizona. The district is about 21 miles long and 7 miles wide and is situated within Tertiary Volcanics of the Black Mountains. Gold was first discovered at Oatman in 1863 in the Moss Vein and subsequent finds in other locations (Gold Road Vein, Tom Reid Vein) led to the development of a town of 10,000 at Oatman after about 1916. Production ceased in the district in 1942 after producing some 2.2 million ounces of gold and 0.8 million ounces of silver.

Oatman was chosen as an Hyperion validation site because of the suite of minerals present (argillic, phyllic and propylitic), its semi-arid nature, being an historic mining center, the existence of appropriate supporting AVIRIS and HyMap data sets and previous mineral mapping research conducted to validate CSIRO ARIES simulation results (Marsh and McKeon, 1983; Huntington et al., 1988; Huntington et al., 1989; Huntington and Boardman, 1995).

The regional geology consists of a thick sequence of Tertiary sub-alkaline, intermediate and silicic volcanic rocks which have been intruded by two epizonal plutons. The Black Mountains are a typical Basin and Range, fault-bounded, Tertiary volcanic sequence composed of trachyte, latite, rhyolite and basalt (Thorson, 1971; Clifton et al., 1980). Oatman lies at the center of a trachyte, latite, rhyolite volcanic complex which contains at least one resurgent caldera. The orebodies are typically low sulfur, epithermal, quartz-calcite +/- adularia lode deposits. Ore deposition has occurred along faults that radiate from a common point within the complex.

An intense and pervasive argillic alteration is evident in the center of the Hyperion study area. Thorson has interpreted this to be a late stage phase of the Moss Porphyry intrusion which has affected both the Lower and Middle Volcanics. More recent studies by Clifton et al. (1980) indicate that the argillic alteration is centered around a previously unmapped rhyolite center located on the eastern margin of the Moss Porphyry. The orebodies of the district occupy dilatant zones within faults structures resulting from dip-slip and strike-slip movements along irregular fault planes. They vary from tabular fissure fillings to complex stockworks of broken, vertically oriented latite slabs separated by quartz calcite veins ranging from an inch to 15 feet wide. Most of these mineralized fractures have a generally similar NW-E orientation, though variations in these trends can be the all important loci for liberalization. In addition to the pervasive argillic alteration there is also significant wall rock alteration which delineates all known ore deposits in the district.

Marsh and McKeon (1983), conclude that there are four distinct alteration assemblages at Oatman which may be directly or indirectly related to the mineralization. These are:

1. pervasive argillic alteration that is characterized by the formation of alunite and sericite (muscovite);

2. spatially restricted, phyllic wall rock alteration which is characterized by the presence of illite. This alteration style extends above the orebodies to the surface in the central district and may coalesce with zones from adjacent veins to form a wider, potentially more visible surface signature;
3. propylitic alteration which introduces chlorite, calcite and epidote into the wall rock;
4. silicification of the wall rock characterized by the introduction of quartz along microfractures.

The above mineralogy and structural control of alteration provides an excellent reference against which to compare and judge the mineralogical mapping capabilities of Hyperion since most of the minerals described should be within the scope of its recognition capabilities.

Other Sites: The November launch of Hyperion and the desire to quickly produce results under optimum acquisition conditions dictated that we acquire data for selected additional southern hemisphere sites. Accordingly, AIG added sites in Australia, New Zealand and Argentina to assist with early Hyperion validation. An AVIRIS data acquisition opportunity during February 2001; AVIRIS deployment to Argentina, also provided the opportunity to collect EO-1 Hyperion support data at a southern hemisphere location coincident with Hyperion data collections. While AIG hasn't conducted any previous mapping at these specific sites, we have proposed to team with other scientists cognizant of site geology (CSIRO for Australia and Perry Remote Sensing (PRS) and a major mining company for Argentina) to assist with evaluation and validation of these data. We have also added an additional site, Makhtesh Ramon, Israel, to take advantage of expertise at Tel Aviv University (Dr. Eyal Ben-Dor) and existing ground and hyperspectral measurements for Hyperion validation. We anticipate that depending upon site coverage and performance, the Hyperion data will provide additional information valuable for geologic understanding of these areas.

5.0 Analysis Example

The NGM site represents the best-case example of a well documented geologic site for Hyperion geologic validation, with both detailed ground information and multiple hyperspectral datasets available. Repeated overflights of the NGM site with a variety of remote sensing instruments were arranged from 1982 through 1999 to evaluate remote sensing technology for resource assessment and to develop advanced analysis methodologies. Remote sensing data available for the NGM site include Landsat MSS and TM, Thermal Infrared Multispectral Scanner (TIMS), MODIS/ASTER (MODIS) Airborne Simulator, JPL Airborne Synthetic Aperture Radar (AIRSAR) and SIR-C. Imaging spectrometer (hyperspectral) data flown for the NGM site include GER Spectral Profiler (1982), Airborne Imaging Spectrometer (AIS) (1984 - 1986), Airborne Visible/Infrared Imaging Spectrometer (AVIRIS) (1987, 1989, 1992, 1994, 1995), Low Altitude AVIRIS (1998), and HyMap (1999). Table 2 summarizes the characteristics of selected datasets and for the planned EO-1 Hyperion.

Table 2: Data acquired and planned for the NGM site, 1982 - 2001

Instrument/Data	Date	Spatial Res.	No. Bands/Spectral Res	SWIR SNR
GER Profiler	1982	20 m	64/~8 nm	500:1
AIS	1984-1986	11-14 m	128/~9.3 nm	~20:1
AVIRIS	1987	20 m	224/~10 nm	15:1
AVIRIS	1989	20 m	224/~10 nm	50:1
AVIRIS	1992	20 m	224/~10 nm	100:1
AVIRIS	1994	20 m	224/~10 nm	100:1
AVIRIS	1995	20 m	224/~10 nm	400:1
AVIRIS	1998	2.4 m	224/~10 nm	400:1
HyMap	1999	3.7 m	126/~17 nm	>500:1+
MASTER	1999	4.3 m	50 (6 SWIR)/~50 – 70 nm	~450:1
EO-1 Hyperion (planned)	2001	30 m	220/~10 nm	50:1

The Mineral Mapping Process: AIG plans to apply the following well-extablished approach to mineral mapping using hyperspectral data to the Hyperion data. These methods have been tested extensively using AVIRIS and other airborne hyperspectral datasets (Boardman and Kruse, 1994; Boardman et al. 1995; Kruse and Huntington 1996; Kruse et al. 1996; and Kruse 1997). The proposed Hyperion data analysis represents the first time that this approach has been applied to satellite hyperspectral datasets.

We believe that hyperspectral data analysis should be cast in the same format as other geophysical data analysis processes. First, the data must be fully calibrated and well characterized. Then instrumental and natural influences on the data, unrelated to our signal of interest, should be modeled and removed via a data reduction step. We use a spectral mixing model to derive the locations and spectral signatures of various key scene components. These derived components, or endmembers, are identified using spectral matching methods and their apparent abundances mapped over the entire hyperspectral scene. Finally, the results are geometrically rectified and map registered (Boardman, 1999). These steps are shown schematically in Figure 2 along with a mapping result. The details of the methodology are described in the following sections.

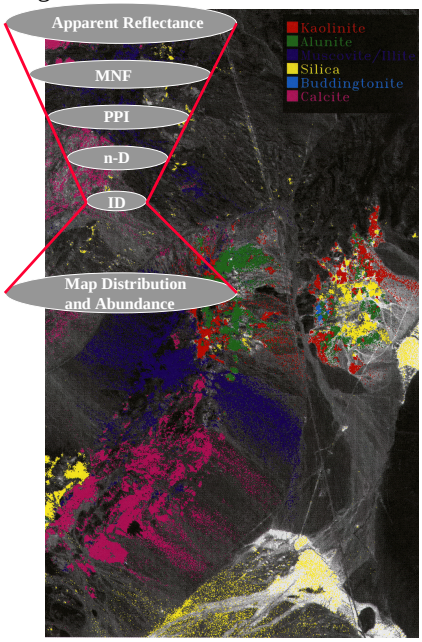

Figure 2: The AIG "Hourglass" method for analysis of hyperspectral data. The underlying image is the result of spectral mapping using "Spectral Feature Fitting', a least-squares fit to endmember spectra, Cuprite, Nevada.

The AIG hyperspectral analysis methodology includes correction of data to apparent reflectance, use of a linear transformation to minimize noise and determine data dimensionality, location of the most spectrally pure pixels, extraction and automated identification of endmember spectra, and spatial mapping and abundance estimates for specific image endmembers. The approach is summarized in more detail below and in Boardman and Kruse (1994), Boardman et al. (1995), Kruse and Huntington (1996), Kruse et al. (1996), and Kruse (1997). A key point of this methodology is the reduction of data in both the spectral and spatial dimensions to locate, characterize, and identify a few key endmember spectra that can be used to explain the rest of the hyperspectral dataset. Once these endmembers are selected, then their location and abundances can be mapped from the original data. The methods described here attempt to derive the maximum information from the hyperspectral data themselves, minimizing the reliance on *a priori* or outside information.

Atmospheric Corrections are a Prerequisite for Most Analysis:

Remote sensing measurements of the Earth's surface are strongly influenced by the atmosphere (Goetz et al., 1985). Both scattering and absorption by gases and particulates affect the amount and wavelengths of light reaching the sensors. Absorption by atmospheric gases is dominated by water vapor with smaller

contributions from carbon dioxide, ozone, and other gases (Gao and Goetz, 1990). Strong atmospheric water absorption bands make the atmosphere opaque in many regions (for example the 1.4 and 1.9 µm regions) and only small atmospheric windows are available for terrestrial remote sensing.

One of the most critical steps in most imaging spectrometer data analysis strategies is to convert the data to reflectance, principally so that individual spectra can be compared directly with laboratory or field data for identification. (If comparison to reflectance isn't required, then this step may be eliminated, but for most work, this is a requirement). Ideally, imaging spectrometer data should be calibrated to absolute reflectance using onboard calibration. Onboard calibration, however, is typically not available. In its absence, one method that comes close to achieving this goal is a radiative transfer model-based technique, "ACORN". ACORN is a commercially available atmospheric correction program (see http://www.aigllc.com) that uses the hyperspectral signature and licensed MODTRAN technology to model the atmosphere and produce apparent reflectance data from hyperspectral radiance measurements. MODTRAN is used to derive and estimate the atmospheric properties for the remote sensing data set on a pixel-by-pixel basis. ACORN corrects for water vapor, oxygen, carbon dioxide, methane, and ozone as well as molecular and aerosol scattering. The software automatically assesses and suppresses artifacts caused by spectral calibration mismatch between the measured data and the radiative transfer calculations. Estimated atmospheric properties are used in an inversion from radiance to apparent surface reflectance. This method makes it possible to quantitatively derive physical parameters and analyze data from different regions and different times without *a priori* knowledge. We can also compare and analyze imaging spectrometry data acquired by different instruments, compare to field and laboratory spectral measurements, or to spectra generated using theoretical models. Correction to reflectance is critical for analysis of the Hyperion data.

MNF Transform

The MNF transformation is a linear transformation related to principal components that orders the data according to signal-to-noise-ratio (Green et al., 1988). The MNF transformation is used to partition the data space into two parts: one associated with large eigenvalues and coherent eigenimages, and a second with near-unity eigenvalues and noise-dominated images (Boardman and Kruse, 1994). In general, the higher numbered MNF bands contain progressively lower signal-to-noise.

Pixel Purity Index (PPI)

Based on the above MNF results, the lower order MNF bands are temporarily discarded and only the higher order bands are selected for further processing. These are used in the "Pixel Purity Index" (PPI), processing designed to locate the most spectrally extreme pixels, which pixels typically correspond to mixing endmembers (Boardman et al., 1995). The PPI is computed by repeatedly projecting n-dimensional scatterplots onto a random unit vector. The extreme pixels in each projection are recorded and the total number of times each pixel is marked as extreme is noted. A PPI image is created in which the digital number of each pixel corresponds to the number of times that pixel was recorded as extreme. A histogram of these images shows the distribution of "hits" by the PPI. A threshold is interactively selected using the histogram and used to select only the purest pixels in order to keep the number of pixels to be analyzed to a minimum. These pixels are used as input to an interactive visualization procedure for separation of specific endmembers.

n-Dimensional Visualization

Spectra can be thought of as points in an n-dimensional scatterplot, where n is the number of bands (Boardman, 1993; Boardman et al., 1995). The coordinates of the points in n-space consist of "n" values that are the spectral reflectance values in each band for a given pixel. The distribution of these points in n-space can be used to estimate the number of spectral endmembers and their pure spectral signatures. In two dimensions, if only two endmembers mix, then the mixed pixels will fall in a line in the histogram. The pure endmembers will fall at the two ends of the mixing line. If three endmembers mix, then the mixed pixels will fall inside a triangle, four inside a tetrahedron, and so on. Mixtures of endmembers "fill in" between the endmembers. All mixed spectra are "interior" to the pure endmembers, inside the simplex formed by the endmember vertices, because all the abundances are positive and sum to unity. This "convex set" of mixed pixels can be used to determine how many endmembers are present and to estimate their spectra.

Mapping Methods

AIG uses a variety of mapping methods depending on the data type and the desired results. These include the Spectral Angle Mapper (SAM) Classification, Spectral Unmixing, Spectral Feature Fitting, Matched Filtering, and Mixture-Tuned Matched Filtering. SAM is an automated method for comparing image spectra to individual spectra (Boardman, unpublished data; Kruse et al., 1993a). The algorithm determines the similarity between two spectra by calculating the "spectral angle" between them, treating them as vectors in a space with dimensionality equal to the number of bands.

Spectral mixing is a consequence of the mixing of materials having different spectral properties within a single image pixel. If the scale of the mixing is large (macroscopic), then the mixing occurs in a linear fashion. A simple additive linear model can be used to estimate the abundances of the materials measured by the imaging spectrometer. Each mixed spectrum is a linear combination of the "pure" spectra, each weighted by their fractional abundance within the pixel, a simple averaging (Boardman, 1989).

Spectral Feature Fitting is an absorption-feature-based methodology for comparing the fit of image spectra to selected reference spectra using a least-squares technique (Kruse et al., 1993b; Kruse and Lefkoff, 1999). This is similar to the "Tetracorder" algorithm developed by the USGS (Clark et al., 1990; Clark and Swayze, 1995), but without the expert system. The reference spectra are scaled to match the image spectra after continuum removal from both data sets. The image and reference spectra are compared at each selected wavelength in a least-squares sense and the root mean square (rms) error is determined for each reference spectrum. The results of Spectral Feature Fitting include a scale image and rms image output for each reference spectrum or a combined "fit" (Scale/RMS) image for each reference spectrum. Best matches to the reference spectrum are easily detected by selecting the high fit scores or by using 2-D scatterplots to select areas with low rms and high scale.

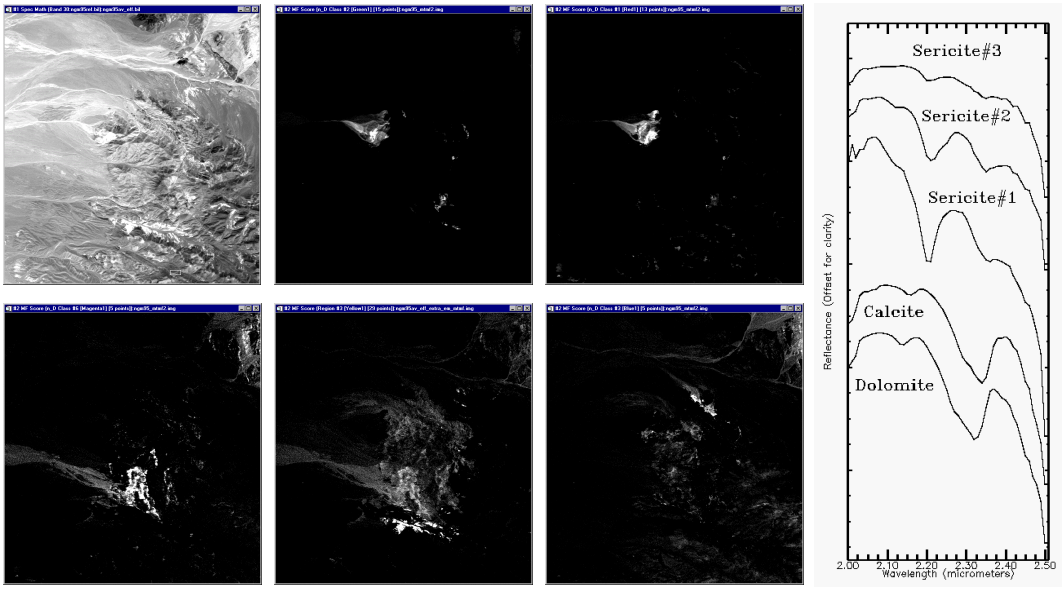

Figure 3: Results for the NGM site showing AVIRIS endmember spectra extracted from the data and identified using a spectral library (right) and Matched Filter mapping results (left). Brighter pixels in the Matched Filter results represent higher abundances.

Mixture-Tuned Matched Filtering is a hybrid method based on the combination of well-known signal processing methodologies and linear mixture theory. The Matched Filter portion of the algorithm maximizes the response of a known endmember and suppressing the response of the composite unknown background (Harsanyi and Chang, 1994) – see Figure 3 below. Mixture-Tuning uses linear spectral mixing theory to constrain the result to feasible mixtures and reduce false alarm rates (Boardman, 1998a). Figure 4 on the following page shows a visual summary of the NGM mapping results for AVIRIS data collected during 2000 in direct support of Hyperion validation

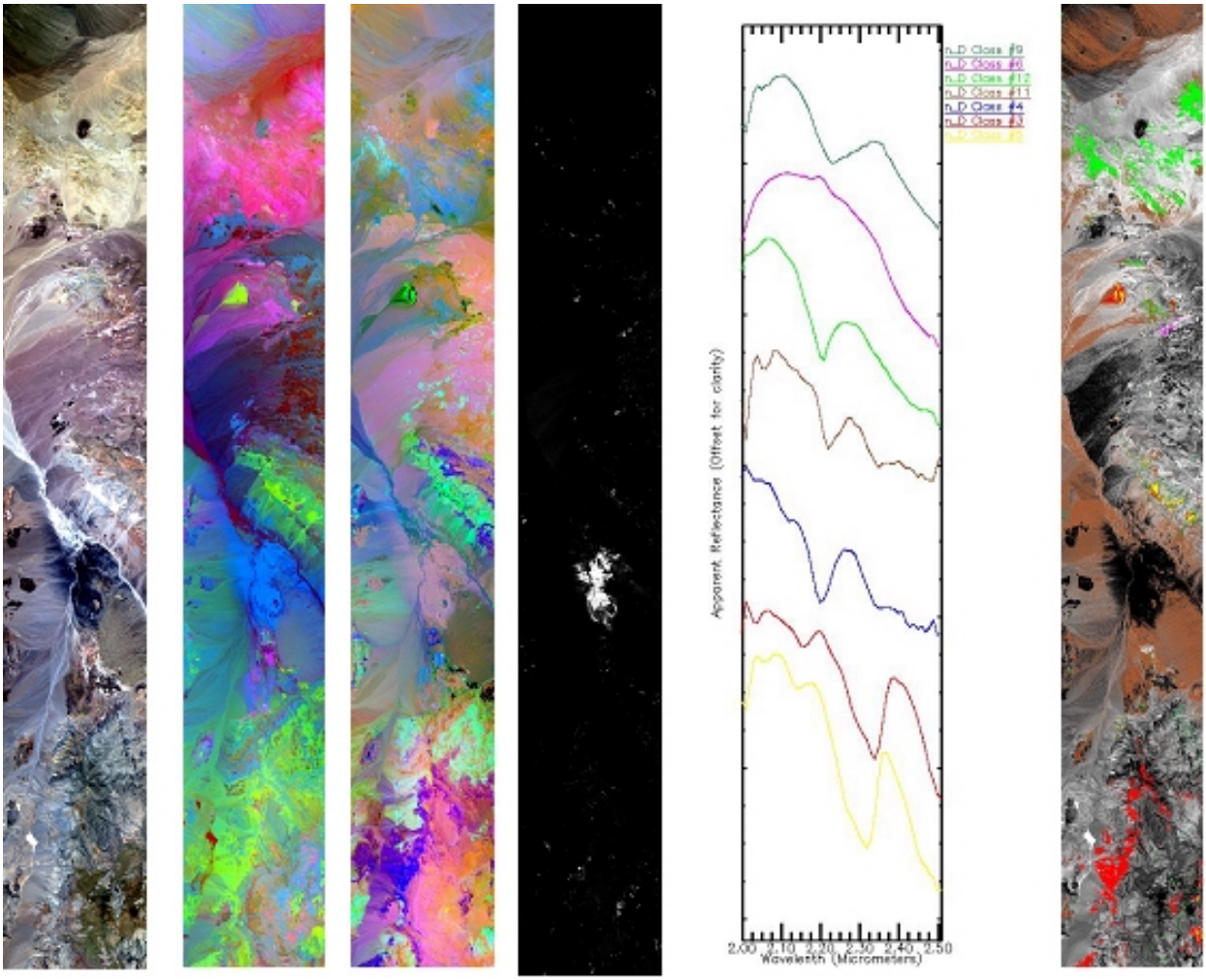

Figure 4: Images and spectra summarizing the AIG approach to analysis of Hyperion data. Images from left to right are: AVIRIS true color image, MNF bands 1, 2, 3 (RGB), MNF bands 4, 5, 6 (RGB), PPI image, extracted endmember spectra, SAM mapping result with class colors corresponding to endmember spectra colors (red=calcite, yellow=dolomite, blue=muscovite#1, brown=muscovite#2, green=muscovite#3, magenta=zeolite, and sea-green=hydrothermal silica).

6.0 Hyperion Validation Plans

Prior to receipt of Hyperion data, we are concentrating on consolidating available AVIRIS and other data for the test sites, compiling mineral maps, and simulating Hyperion performance. We plan to work with the AVIRIS data to generate simulations with Hyperion's 30 meter pixel size and approximate 100:1 (VNIR) and 50:1 (SWIR) signal-to-noise ratios (SNR). We expect that these simulations will answer some of the questions about how Hyperion will perform against our test sites and specific questions of interest for mapping mineral deposits. Questions to be answered include: 1. how will the 30m spatial resolution effect detection of small (vein) occurrences; will subpixel

detection and mapping methods allow us to map critical areas? 2. how will the reduced SNR of Hyperion (as compared to AVIRIS) effect our mapping capabilities?

We have done some direct comparison of the Signal-to-Noise-Ratio (SNR) effects utilizing AVIRIS. AVIRIS data acquired over the period 1989 – 1995 on the ER-2 platform for the NGM site share 20m spatial resolution and approximately 10nm spectral resolution. All data were corrected to apparent reflectance using ATREM (CSES, 1999). SNR for these datasets were not directly computed. Instead, reported SNR for the acquisition year SNR under standard AVIRIS radiance conditions (50% reflectance, solar noon) were used to select a range of representative data. Reported SNR for these data are approximately: 50:1 (1989), 100:1 (1992), and 400:1 (1995) for the D spectrometer (2.0 – 2.5 μm) as reported by Green et al., 1990, 1993, 1996. The 1995 data were also corrected for residual systematic errors utilizing the EFFORT method of Boardman (1998b). This correction is only possible on the 1995 data because of its exceptional signal-to-noise characteristics. Single-pixel spectra were extracted from the data for two key materials at the NGM site; carbonates, and sericitic alteration. Figure 5 shows spectral plots of the 1989, 1992, and 1995 reflectance spectra for calcite and dolomite endmembers. Though there are obvious SNR differences, the position of the diagnostic spectral feature for dolomite near 2.32 mm could be separated from the spectral feature for calcite at all SNR levels. At the 50:1 SNR, there is some calcite/dolomite confusion. It should be clear, that any automated feature-based method will have difficulty picking out the specific absorption features at the lower SNR levels. Figure 6 shows a comparison of spectral plots for single-pixels for sericitic alteration identified at the NGM site. First, note that for both the 1989 and 1992 cases, only two different sericite varieties were distinguishable. The 1995 data indicate that there are actually three distinct species of sericite at the NGM site based on the position of the main feature near 2.2 μm, a fact verified by microprobe analysis (Kruse et al., 1999).

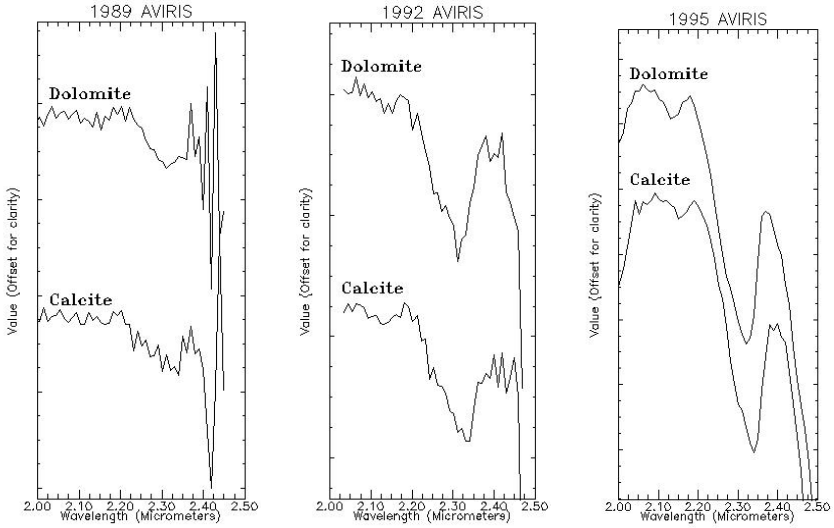

Figure 5: Comparison of 1989 (left), 1992 (center), and 1995 (right) single-pixel AVIRIS spectra for areas identified as calcite and dolomite at the NGM site (from Kruse, 2000).

Plans for analysis of Hyperion data include correction to apparent reflectance utilizing ACORN and analysis using standardized AIG methodologies described above. Validation efforts will concentrate on verifying Hyperion's spatial and spectral resolution as well as SNR performance. We will then compare the Hyperion analysis results for the various sites to those achieved with AVIRIS as well as ground spectral measurements and mapping to determine the utility of Hyperion for geologic applications.

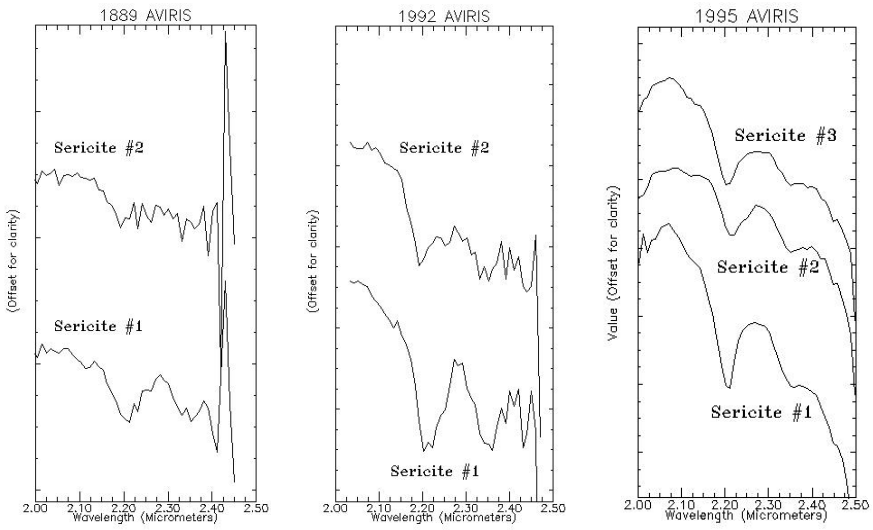

Figure 6 Comparison of 1989 (left), 1992 (center), and 1995 (right) single-pixel AVIRIS spectra for sericitic alteration at the NGM site (from Kruse, 2000).

7.0 Conclusions

We have described our geologic test sites for Hyperion and outlined our analysis approach. The NGM AVIRIS example presented demonstrates the baseline against which the Hyperion data will be judged. This work and other cited references demonstrate that spatial resolution, spectral resolution, and SNR can have dramatic effects on the ability to perform mineral mapping using hyperspectral data. Previous work (Kruse, 2000) indicates that spatial resolution is the key to mapping of detailed, scale-dependent variation. Increasing the pixel size (decreasing the spatial resolution) results in the loss of image detail. There is a tendency to lose small, discrete occurrences of specific materials with larger pixels. The same study indicates that spectral resolution is the key to separation of subtle material differences. Decreasing the spectral resolution results in losses in the ability to distinguish and map fine spectral detail. Coarser spectral resolution can prohibit discrimination and identification of specific minerals. Finally, as shown in Figures 5 and 6, SNR is the key to overall quality of the spectral mapping process. There is decreased capability to define key spectra with decreasing SNR. If the SNR level is inadequate, neither spatial or spectral resolution matters. We expect to validate Hyperion in this context.

Some final comments on expectations for EO-1 Hyperion and future satellite systems: We are NOT expecting Hyperion to perform like 2000 AVIRIS! Hyperion will, however, demonstrate the viability of Satellite Hyperspectral Sensing. A key factor is its potential for site acquisition world-wide. We expect that Hyperion will be useful for geologic mapping on about the level of the 1989 AVIRIS data. Its 30m spatial resolution, 10 nm spectral resolution, and SWIR SNR of 50:1 should produce results similar to those shown for 1989 AVIRIS data in other published work (Kruse, 2000). These capabilities will be combined with airborne systems such as AVIRIS and HyMap to allow scaling of higher spatial and spectral resolution measurements. Future satellite systems should provide sufficient spatial resolution to allow overview coverage (trade off for SNR), spectral resolution around 10 - 20 nm (trade off for SNR), and SNR “as high as possible”.

8.0 Acknowledgements

Collection and analysis of support data being used for this Hyperion validation effort were supported over the years by the U.S. Geological Survey, Colorado School of Mines, NASA/JPL, Center for the Study of Earth from Space (CSES, University of Colorado), and Analytical Imaging and Geophysics LLC. Special thanks are due to the JPL AVIRIS team for their dedication and support. Portions of this manuscript and related research were funded by AIG internal research and development (IR&D) in support of NASA EO-1 Hyperion. The 2000 AVIRIS data and additional funding for this research were provided under AIG’s EO-1 NASA-funded proposal "EVALUATION AND GEOLOGIC VALIDATION OF EO-1 HYPERION”, grant number NCC5-495.

9.0 References Cited

Albers, J. P., and Stewart, J. H., 1972, Geology and mineral deposits of Esmeralda County, Nevada: Nevada Bureau of Mines and Geology Bulletin 78, 80 pages.

Boardman, J. W., 1989, Inversion of imaging spectrometry data using singular value decomposition: in Proceedings, IGARSS '89, 12th Canadian Symposium on Remote Sensing, 4, pp. 2069–2072.

Boardman, J. W., 1993, Automated spectral unmixing of AVIRIS data using convex geometry concepts: in Summaries, Fourth JPL Airborne Geoscience Workshop, JPL Publication 93-26, v. 1, pp. 11–14.

Boardman, J. W., 1998a, Leveraging the high dimensionality of AVIRIS data for improved sub-pixel target unmixing and rejection of false positives: mixture tuned matched filtering, in: Summaries of the Seventh Annual JPL Airborne Geoscience Workshop, Pasadena, CA, p. 55.

Boardman, J. W., 1998b, Post-ATREM polishing of AVIRIS apparent reflectance data using EFFORT: a lesson in accuracy versus precision: in Proceedings of the 8th JPL Airborne Earth Science Workshop: Jet Propulsion Laboratory Publication 99-17, p. 53.

Boardman, J. W., 1999, Precision geocoding of AVIRIS low-altitude data: lessons learned in 1998: in Proceedings of the 8th JPL Airborne Earth Science Workshop: Jet Propulsion Laboratory Publication 99-17, pp. 63–68.

Boardman, J. W., and Kruse, F. A., 1994, Automated spectral analysis: A geological example using AVIRIS data, northern Grapevine Mountains, Nevada: in Proceedings, Tenth Thematic Conference, Geologic Remote Sensing, 9-12 May 1994, San Antonio, Texas, pp. I-407–I-418.

Boardman, J. W., Kruse, F. A., and Green, R. O., 1995, Mapping target signatures via partial unmixing of AVIRIS data: in Summaries, Fifth JPL Airborne Earth Science Workshop, JPL Publication 95-1, v. 1, pp. 23–26.

Clark, R.N. and Swayze, G.A., 1995, Mapping Minerals, Amorphous Materials, Environmental Materials, Vegetation, Water, Ice and Snow, and Other Materials: The USGS Tricorder Algorithm. Summaries of the Fifth Annual JPL Airborne Earth Science Workshop, January 23–26, R.O. Green, Ed., JPL Publication 95-1, pp. 39–40.

Clark, R.N., A.J. Gallagher, and G.A. Swayze, 1990, Material Absorption Band Depth Mapping of Imaging Spectrometer Data Using a Complete Band Shape Least-Squares Fit with Library Reference Spectra: in Proceedings of the Second Airborne Visible/Infrared Imaging Spectrometer (AVIRIS) Workshop. JPL Publication 90-54, pp. 176–186, 1990.

Center for the Study of Earth from Space (CSES), 1999, Atmosphere REMoval Program (ATREM) User's Guide, Version 3.1, Center for the Study of Earth from Space, Boulder, Colorado, 31 pages.

Clifton, C.G., Buchanan, L.J. and Durning, W.P., 1980, Exploration Procedure and Controls of Mineralisation in the Oatman Mining District, Oatman, Arizona: New York, So. Of Mining Engineers of AIME, Reprint, 80-143, 17 pages.

Elvidge, C.D., 1985, Separation of leaf water and mineral absorption in the 2.2 micrometre Thematic Mapper band: Unpublished Ph.D. dissertation, Stanford University, 182 pages.

Gao B. and Goetz, A. F. H., 1990, "Column atmospheric water vapor and vegetation liquid water retrievals from airborne imaging spectrometer data." Journal of Geophysical Research, 95(D-4): pp. 3549–3564.

Goetz, A. F. H., Vane, G., Solomon, J. E., and Rock, B. N., 1985, Imaging spectrometry for earth remote sensing: Science, 228, pp. 1147–1153.

Green, A. A., Berman, M., Switzer, B., and Craig, M. D., 1988, A transformation for ordering multispectral data in terms of image quality with implications for noise removal: IEEE Transactions on Geoscience and Remote Sensing, v. 26, no. 1, pp. 65–74.

Green, R. O., Conel, J. E., Carrere, V., Bruegge, C. J., Margolis, J. S., Rast, M., and Hoover, G., 1990, Determination of the in flight spectral and radiometric characteristics of the Airborne Visible/Infrared Imaging Spectrometer (AVIRIS): in Proceedings, 2nd Airborne Visible/Infrared Imaging Spectrometer (AVIRIS) workshop, JPL Publication 90-54, pp. 15–34.

Green, R. O., Conel, J. E., Helmlinger, M., van den Bosch, J., Chovit, C. and Chrien, T., 1993, Inflight calibration of AVIRIS in 1992 and 1993: in Summaries, 4th Annual JPL Airborne Geoscience Workshop, JPL Publication 93-26, pp. 69–72.

Green, R. O., Conel, J. E., Margolis, J., Chovit, C., and Faust, J., 1996, In flight calibration and validation of the Airborne Visible/Infrared Imaging Spectrometer (AVIRIS): in Proceedings, 6th Airborne Visible/Infrared Imaging Spectrometer (AVIRIS) workshop, JPL Publication 96-4, v. 1, pp. 115–126.

Harsanyi, J. C., and Chang, C. I., 1994, Hyperspectral image classification and dimensionality reduction: An orthogonal subspace projection approach: IEEE Trans. Geosci. and Remote Sens., v. 32, pp. 779–785.

Hudson, D. M., 1984, Geology of the Comstock District, Storey County, Nevada: Report prepared for United Mining Company of Nevada, Virginia City, Nevada, 29 pages.

Huntington, J.F. and Boardman, J.W., 1995, Semi-quantitative Mineralogical and Geological Mapping with 1995 AVIRIS Data, Proc. Spectral Sensing Research '95, ISSSR, Published by the AGPS, 26 Nov–1 Dec, 1995, Melbourne, Australia.

Huntington, J.F., Green, A.A. and Craig, M.D., 1989. Identification - the Goal Beyond Discrimination. The status of mineral and lithological identification from high resolution spectrometer data: Examples and challenges. Invited Keynote paper. In "Remote Sensing: An Economic Tool for the Nineties", IGARSS '89, 12th Canadian Symposium on Remote Sensing, Vancouver, 10-14 July, 1989, Vol.1, pp. 6–11. IEEE#89CH2768-0

Huntington, J.F., Green, A.A., and Craig, M.D., 1988, Mineral and Lithological Mapping with the GER 64 Band Scanner: US and Australian Examples. Poster and presented paper, 6th Thematic Conf. on "Remote Sensing for Mineral Exploration", Houston Texas, May 16-19 1988 pp. 39–40.

Hutsinpiller, A., 1988, Discrimination of Hydrothermal Alteration Mineral Assemblages at Virginia City, Nevada, Using the Airborne Imaging Spectrometer. Remote Sensing of Environment, Vol. 24, pp.53–66.

Kruse, F. A., 1988, Use of Airborne Imaging Spectrometer data to map minerals associated with hydrothermally altered rocks in the northern Grapevine Mountains, Nevada and California: Remote Sensing of Environment, v. 24, no. 1, pp. 31–51.

Kruse, F. A., 1997, Regional Geologic Mapping Along the Colorado Front Range from Ft Collins to Denver Using the Airborne Visible/Infrared Imaging Spectrometer (AVIRIS): in proceedings, 12th Thematic Conference, Applied Geologic Remote Sensing, 17-19 November 1997, Environmental Research Institute of Michigan (ERIM), Ann Arbor, MI, pp. II-91–II-98.

Kruse, F. A., 2000, The effects of spatial resolution, spectral resolution, and SNR on geologic mapping using hyperspectral data, northern Grapevine Mountains, Nevada: in Proceedings of the 9th JPL Airborne Earth Science Workshop: Jet Propulsion Laboratory Publication.

Kruse, F. A., and Huntington, J. H., 1996, The 1995 Geology AVIRIS Group Shoot: in Proceedings, 6th JPL Airborne Earth Science Workshop: Jet Propulsion Laboratory Publication 96-4, v. 1, pp. 155–166.

Kruse, F. A., and Lefkoff, A. B., 1999, Analysis of Spectral Data of Manmade Materials, Military Targets, and Background Using an Expert System Based Approach**:** In Proceedings, ISSSR'99, 31 October – 4 November 1999, Las Vegas, Nevada.

Kruse, F. A., Huntington, J. H., and Green, R. O, 1996, Results from the 1995 AVIRIS Geology Group Shoot: in Proceedings, 2nd International Airborne Remote Sensing Conference and Exhibition: Environmental Research Institute of Michigan (ERIM), Ann Arbor, v. I, pp. I-211–I-220.

Kruse, F. A., Lefkoff, A. B., Boardman, J. B., Heidebrecht, K. B., Shapiro, A. T., Barloon, P. J., and Goetz, A. F. H., 1993a, The Spectral Image Processing System (SIPS) - Interactive Visualization and Analysis of Imaging Spectrometer Data: Remote Sensing of Environment, Special issue on AVIRIS, May-June 1993, v. 44, pp. 145–163.

Kruse, F. A., Lefkoff, A. B., and Dietz, J. B., 1993b, Expert System-Based Mineral Mapping in northern Death Valley, California/Nevada using the Airborne Visible/Infrared Imaging Spectrometer (AVIRIS): Remote Sensing of Environment, Special issue on AVIRIS, May-June 1993, v. 44, pp. 309–336.

Kruse, F. A., Boardman, J. W., and Huntington, J. F., 1999, Fifteen Years of Hyperspectral Data: northern Grapevine Mountains, Nevada: in Proceedings of the 8th JPL Airborne Earth Science Workshop: Jet Propulsion Laboratory Publication, JPL Publication 99-17, pp. 247–258.

Marsh, S.E. and McKeon, J.B., 1983, Integrated Analysis of High-Resolution Field and Airborne Spectroradiometer Data for Alteration Mapping, Econ. Geol. Vol.78, No.4, pp.618-632.

Moring, B., 1986, Reconnaissance surficial geologic map of northern Death Valley, California and Nevada: U. S. Geological Survey Miscellaneous Field Studies Map MF-1770, 1:62,500, 1 sheet.

Thorson, J.P., 1971, Igneous Petrology of the Oatman Mining District, Mohave County, Arizona, Unpublished Ph.D dissertation, Uni. California, Santa Barbara, 189 pages.

Thompson, J.V., 1956, Geology of the Virginia City Quadrangle, Nevada, USGS Bull. 1042-C, 75 pages.

Whitebread, D.H., 1976, Alteration and Geochemistry of Tertiary Volcanic Rocks in Parts of the Virginia City Quadrangle, Nevada, US Geological Survey Professional Paper No. 936, 43 pages.

Wrucke, C. T., Werschkey, R. S., Raines, G. L., Blakely, R. J., Hoover, D. B, and Miller, M. S., 1984, Mineral resources and mineral resource potential of the Little Sand Spring Wilderness Study Area, Inyo County, California: U. S. Geological Survey Open File Report 84-557, 20 pages.